Review of Scientific Instruments ARTICLE scitation.org/journal/rsi

Short-pulse KrF amplifier using spatially tunable x-ray preionization

Cite as: Rev. Sci. Instrum. 91, 043001 (2020); doi: 10.1063/1.5143202
Submitted: 20 December 2019 • Accepted: 8 April 2020 •
Published Online: 29 April 2020

S. Szatmári[1,2,a)]

AFFILIATIONS

[1] Department of Experimental Physics, University of Szeged, Dóm tér 9, H-6720 Szeged, Hungary
[2] Department of Photonics and Laser Research, Interdisciplinary Excellence Centre, University of Szeged, Dugonics tér 13, H-6720 Szeged, Hungary

[a)] **Author to whom correspondence should be addressed:** expphys@physx.u-szeged.hu

ABSTRACT

The small saturation energy density of excimers requires amplifiers of large cross sections for amplification of short pulses of already medium power. Homogeneous excitation of large volumes of fluorine-based gas mixtures by discharge pumping is a critical interplay of the properties of both pumping and preionization, generally necessitating an intense spatially and temporally controlled x-ray preionization. In the present realization, the stringent intensity requirements of preionization are fulfilled by reducing the pulse duration of the x-ray flash to ~16 ns and by positioning the x-ray source in the near vicinity of the active volume. It is proven both theoretically and experimentally that by proper choice of the positions of two cylindrical x-ray guns, the spatial distribution of preionization can be tuned to (and around) the optimum distribution. In this way, the spatial distribution of the discharge can also be controlled, giving a practical method to compensate for eventual inhomogenities of the E-field of excitation and to tune the discharge to the desired geometry. In this paper, design considerations and experimental realization of a KrF excimer amplifier of ~5 × 4 cm^2 cross section and a spatially tunable x-ray preionization are presented.

I. INTRODUCTION

In view of the recent progress of IR solid-state laser systems, high-brightness ultraviolet (UV) excimer lasers can be regarded as complementary sources. Their main advantage occurs in those experiments where high photon energy, optimum spatial concentration, and/or efficient conversion of the pulse energy to radiation of even shorter wavelength are needed.[1,2] At present, the performance of short-pulse UV systems is definitely below that of the IR solid-state systems as the maximum peak power is concerned.[3–6] This is primarily due to the difficulties associated with the construction of short-pulse UV amplifiers[1,2] and with the inherently limited energy extraction from excimer amplifiers of short energy storage time.[1,7]

Present high-brightness UV lasers are double wavelength systems,[1,8] where the short-pulses of optimum temporal and spatial quality are generated and preamplified in the IR or in the visible range, and the UV wavelength is reached by frequency upconversion, where excimer amplifiers are used to boost up the power typically to the TW level.[1,2,9,10]

Excimers are ideal four-level systems allowing very efficient operation even in the UV for pulses longer than the storage (or pumping) time. However, they exhibit moderate extraction efficiency for shorter pulses because of the relatively short (several ns) storage time compared to the accessible pumping times (several times 10 ns or more). It also means that for a given value of the accessible optical energy (called momentarily stored energy), $E_m = \varepsilon_{sat} g_0 l A$ (where ε_{sat} is the saturation energy density, g_0 is the small signal gain coefficient, l and A are the length and the cross section of the active medium, respectively), and significantly more energy has to be pumped in (or through) the active medium.

The saturation energy density of excimers is very low compared to the solid-state systems, typically in the range of several mJ/cm^2. In KrF power amplifiers—due to the inherent presence of nonsaturable absorption in the active medium—the optimum operation both for efficiency and contrast is a critical function of the energy density.[1,11] Both requirements can never be fulfilled at the same time; one can only have a trade-off, when the energy density is set to $\varepsilon_{opt} \approx 2.2$ and

$\varepsilon_{sat} \approx 4.5$ mJ/cm^2.[1,2,11,12] This condition—together with the low value of ε_{sat}[13]—however, requires large amplifier cross sections already for moderate output energies.

Due to these requirements, the pumping of excimer gain modules can only be realized by an efficient and temporally short pumping mechanism capable of homogeneously exciting a large volume of a large cross section in a short time comparable to the energy storage time. E-beam pumping can, in principle, fulfill these conditions, but its use leads to a complex and bulky design. Discharge pumping of excimers is more straightforward for many practical reasons; however, special considerations and corresponding steps are needed to homogeneously deposit a large amount of electric energy into a gas-filled volume of well-defined dimensions in a very short time.[9,10,14,15]

It is known from former gain dynamic studies[1,13] that it is only KrF and ArF that act as a real four-level system when short-pulse amplification is needed, allowing good access to the momentarily stored energy. On the other hand, these are just the excimers where homogeneous excitation of the initial fluorine-based gas mixture is the most critical; special measures are needed to ensure arc-free, homogeneous excitation of large volumes.[16] One needs a fast rising, temporally clean electric pulse to produce a highly uniform electric field together with a fast and efficient preionization of the gas characterized by a similarly uniform spatial distribution of the generated electrons (ions). Due to the strong halogen attachment, their effective lifetime is shortened to several times 10 ns, which necessitates a comparably short and intense preionization process, precisely synchronized to the main pumping pulse.

The requirements for the necessary cross section of the amplifier can be relaxed by the use of the so-called off-axis amplification scheme,[12] which also relaxes the requirements concerning the optimum cross-sectional shape of the discharge. From the optical point of view, a circular cross section is ideal, necessitating a discharge cross section of w/d ≈ 1 aspect ratio (where w is the width of the discharge and d is the separation between the electrodes). It is pointed out in Ref. 1 that with the use of the off-axis scheme, the aspect ratio can be decreased down to w/d ≈ 0.3. Such discharges are more stable, relatively simple to create with standard charging circuits, and technically simple UV preionization.[8,10,15] On the other hand, the increase in the aspect ratio is still desirable for two reasons; this necessarily leads to the increase in the pumped volume resulting in increased momentarily stored energy; moreover—because of the presence of nonsaturable absorption of the gas mixture—it minimizes the absorbing unpumped volume seen by the short signal pulse. A discharge of a large cross section and of aspect ratio, however, necessitates the use of x-ray preionization, which is known to be capable of homogeneously ionizing large volumes.[14,16–19]

In the case of x-ray preionization of discharge-pumped excimer gain modules, a large penetration depth (small absorption coefficient) of the x-ray radiation in the gas mixture is a necessary condition to achieve spatially uniform ionization. (The spatial dependence of the x-ray field can also be neglected if the radiation source is relatively far from the volume to be ionized.) The small absorption, however, minimizes the absorbed energy. This sets stringent requirements for the strength of the x-ray source. Because of the very fast (a few times 10 ns) recombinations of the electrons in the fluorine-based gas mixtures, preionization must be comparably fast, necessitating an intense x-ray source of similar or shorter duration. This very stringent requirement for the intensity (not for the dose!) of the x-ray radiation is one of the main reasons, why in former publications no saturation of the preionization is reached;[18] even in some cases, the necessary density of electrons ($n \approx 10^6$–10^8 1/cm^3[16]) is hardly produced.

A possible way to increase the intensity of x rays is to decrease the spatial separation of the x-ray source and the gas volume to be preionized. This, however, generally leads to a spatially inhomogeneous intensity distribution, when the distance of the x-ray source becomes comparable to the dimensions of the volume to be preionized. This latter condition can only be relaxed by the use of spatially distributed (surface-emitting) x-ray sources,[16,18,19] where the exact control on the spatial distribution of the emission is absolutely necessary to maintain well-defined spatial distribution of the x rays in the gas volume.

Former investigations showed that the spatial distribution of the discharge is the critical interplay of both the E-field and the preionization.[20] For a given E-field distribution, this makes, in principle, possible to fine-tune the discharge geometry by controlling the spatial characteristics of preionization, as also shown in Ref. 20. In that paper, a novel technique is introduced (and experimentally verified) for improving the uniformity of the discharge by the proper control of the spatial distribution of the preionizing x-ray field. This is realized by proper masking/by spatially dependent attenuation of the radiation of a single external x-ray source.

Based on the geometrical requirements imposed by the planned volume of ~40 × 5 × 5 cm^3 to be preionized, and by our former experimental experience associated with the development of pencil-like, pulsed, x-ray sources of reflective geometry, in this paper design considerations and first results are reported for a large aperture, short-pulse KrF amplifier module, preionized by a spatially tunable, twin x-ray gun.

II. EXPERIMENTAL REALIZATION

A. X-ray preionizer/driving circuit

As it is described in the Introduction, a spatially elongated, intense x-ray source of short pulse duration is mandatory for efficient preionization of a transversally pumped KrF excimer gas mixture. For practical reasons (described later), our development was concentrated on the realization of a twin, cylindrical x-ray gun powered by a common power supply. With regard to the pulsed operation required here, a pulsed plasma electron source was chosen as the (cold) cathode of the x-ray gun.[21] Among the possible cathode designs, the so-called carbon-epoxy capillary cathode design was selected, offering very high (>300 A/cm^2) current densities and a very simple, practical diode design.[22] The realization of the x-ray gun is shown in Fig. 1. The diode is formed by a cylindrical tungsten anode of 6.3 mm diameter and 50 cm length, positioned in the center of a glass tube of 40 mm diameter and 1.5 mm wall thickness. This anode is supported at both ends of the tube by insulators far away from the ends of the somewhat shorter cathode of ~40 cm length. The cathode is an array of carbon-epoxy capillaries (Van Dijk Pultrusion Products) of 1.5 mm/0.7 mm outer/inner diameters, respectively. These capillaries are uniformly distributed and glued to an aluminum holder of 6 mm diameter. The period

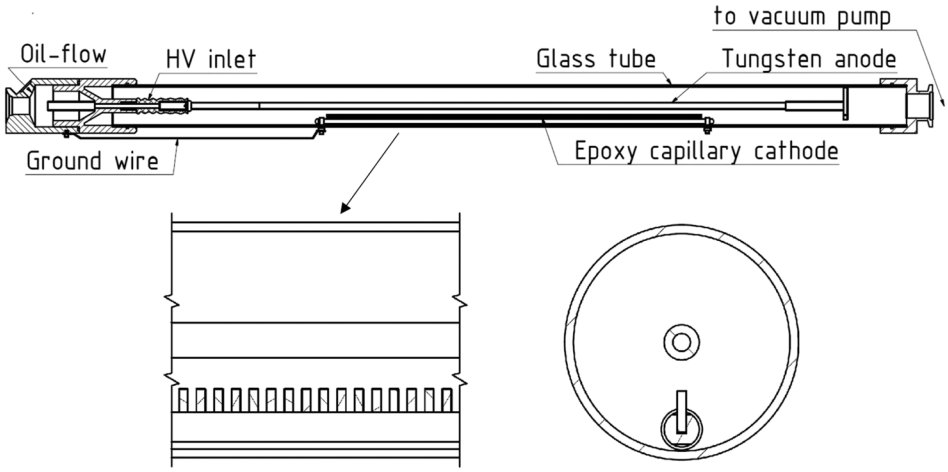

FIG. 1. Schematics of the cold-cathode x-ray gun of cylindrical geometry.

between the capillaries is 3 mm. A detailed structure of the cold-cathode diode of the x-ray gun is also shown in Fig. 1 (see the enlarged—side and cross-sectional—view of the central portion of the tube). The cathode is connected to the ground potential through holes of the glass tube at both ends of the cathode. The anode is fed by a ~100 kV positive voltage pulse at one end of the evacuated tube, which is directly connected to an oil-filled cylindrical pulse forming line (which connects at the same time the x-ray gun to the pulsed power supply). This design relaxes the isolation issues, necessarily to be considered when driving such a miniature design by 100 kV-s.

It is known that pulsed plasma electron sources are efficient and capable of producing a stable and uniform cross-sectional current density distribution, if the rise of the electric field surpasses a given limit ($dE/dt \geq 10^{13}$ V/cm s).[22] For this reason and for the expected very strong attachment of the electrons by the fluorine in the gas mix, the generation of an electric pulse of very short (<50 ns) duration, and of even shorter rise time has been proven necessary to drive the two x-ray guns.

The circuit diagram of the pulsed power supply is shown in Fig. 2. Here, an LP189 thyratron—used in a grounded cathode mode—switches the charge of C (=12 nF each) capacitors to the two transformers (Tr). The toroidal core of the transformers is made of a soft ($\mu_r \approx 3–5 \times 10^3$) magnetic material (Vitroperm 250F, VAC Vacuumschmelze GmbH) exhibiting high saturation flux density ($B_{sat} \approx 1.2$T) and very small core loss, thus, ensuring efficient transfer of considerable electric energy with limited core mass in a single shot. All these components were immersed in insulating oil. The cylindrical oil container of the transformers serves as a one-turn primary winding to minimize its scatter inductance and to ensure homogeneous magnetization of the core. The secondary winding is formed by three identical coils of four windings each, positioned symmetrically along the core. Using this arrangement, both diodes could be driven by synchronized >100 kV electric pulses of ~30 ns duration and ~20 ns rise time.

The temporal behavior of the electric pulse—measured at the input of the pulse forming line by a built-in voltage probe—is shown in Fig. 3 (curve U). Curve I is the corresponding current, measured at the same point by a Rogowski pick-up coil.

Optimum matching of the impedance of the diode to that of the driving circuit is of great importance to get efficient operation. The impedance of the diode is basically determined by the number and by the emission rate of the carbon fibers. The latter one turned to show a long-term drift in the "drive-in" period, attributed to the change in the microscopic surface morphology in the first period of operation. This, however, can be compensated by adjusting the dE/dt value (e.g., by changing the anode–cathode separation) to a required value of the emission rate, which corresponds to optimum impedance matching. In our case—having 118 pieces of fibers in each diode—a gap separation of d ≈ 3 mm resulted in optimum operation in the "stationary driven-in" condition. With the given values of the driving voltage of U = 100 kV and its rise time of T = 20 ns, the 3 mm gap separation resulted in a rise of the electric field $dE/dt \approx 1.7 \times 10^{13}$ V/cms, sufficiently surpassing the threshold conditions for the efficient operation of plasma electron sources.[22]

The dose and the temporal behavior of the x-ray radiation generated by one diode were determined by an ionization chamber

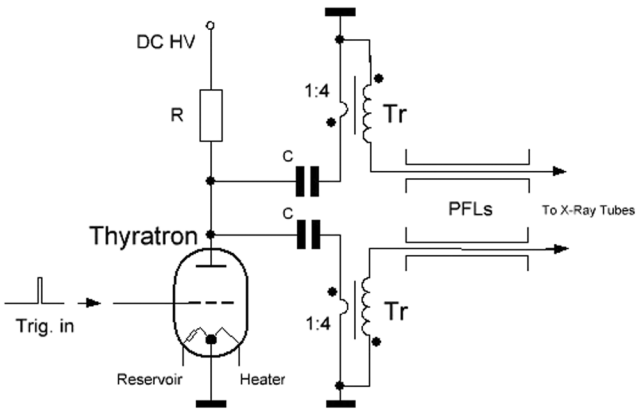

FIG. 2. Circuit diagram of the pulsed power supply for synchronized pumping of two x-ray guns.

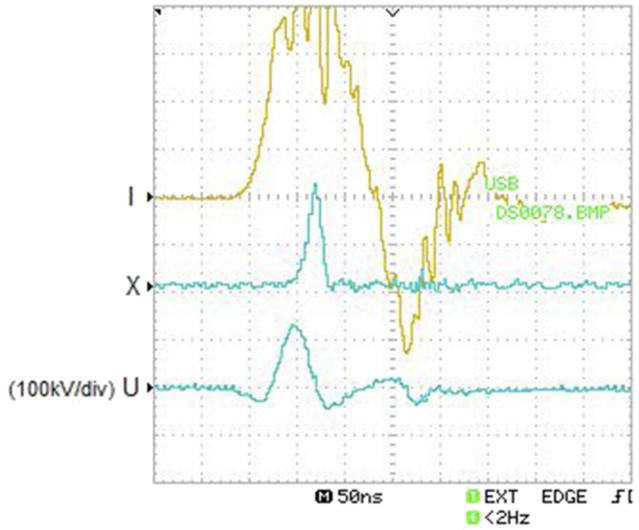

FIG. 3. Temporal behavior of the current (I), the voltage (U), and the x-ray pulse (X) of the preionizer.

and by a fast silicon-diode amplifier arrangement, both positioned 10 cm away from the cylindrical anode of the x-ray gun. For the absolute measurement of the x-ray dose, ions—accelerated by a 1.2 kV DC potential in an air filled ionization chamber of 25 × 25 × 20 cm^3 dimension—were collected and amplified using an LF356-based charge amplifier. The calculated and measured response of this device was 1.5 V ms/mR. For temporal measurements, an RD15 silicon photodiode (OSI Optoelectronics) —followed by an LM7171-based current-to-voltage converter—was used. In the case of x-ray detection, the front surface of the diode was shielded by a thin aluminum foil, which—together with the metal housing of the detector-amplifier unit—ensured efficient suppression of the electromagnetic interference (EMI). For the measurement of the temporal resolution of this unit, the photodiode was directly illuminated by a subpicosecond light-pulse, and the temporal width of the electric pulse leaving the output of the amplifier was measured and regarded as the temporal resolution. A maximum temporal resolution of 6 ns is reached. Depending on the feedback loop of the circuit, the sensitivity could be increased, however, at the expense of the temporal resolution. As an optimum trade-off, a detection system of 14 V ns/mR response with 10 ns resolution was applied in our later measurements. The x-ray dose (for one x-ray gun) was measured to 11 mR, and the FWHM of the x-ray pulse was 16 ns. The oscilloscope trace of the latter measurement is shown in Fig. 3 by curve X. The 16 ns temporal width for the x-ray pulse is obtained through deconvolution of the measured value by the 10 ns resolution of the detection system. Note that the very short duration of x rays compared to the former approaches (where much longer pulses of several hundred ns duration are normally used for the generation of short living electrons) is a real advantage in minimizing the necessary electric energy while reaching even larger electron density.

This is explained by the following numerical example. Based on the measurement data of Ref. 18, an x-ray pulse of ~30 mR dose (and 400 ns duration) creates an electron density of 3 × 10^8 1/cm^3, 10^7 1/cm^3, and 10^8 1/cm^3 in 150 mbar Kr, 2 bars He, and 3 bars Ne, respectively. Without the effect of the F_2 attachment, these electron densities (or in the case of gas mixtures the sum of them) are available over a long period of the recombination time. However, in the presence of F_2, the effective lifetime of electrons is drastically reduced to the 10 ns time scale.

It means that by using a comparably short x-ray pulse (of the same, 30 mR dose), electron densities of 3 × 10^8 1/cm^3 and 4 × 10^8 1/cm^3 can be reached for Xe/He and Xe/Ne-based fluorine gas mixtures, respectively. On the other hand, if one uses a 400 ns long x-ray pulse (as in many former experiments), the electron density remains definitely below 10^7 1/cm^3. In our case—considering the 16 ns duration of the x-ray pulse and the ~20 mR dose of the two x-ray guns—an electron density of ≥10^8 1/cm^3 is calculated. This is above the limit of the efficient preionization of both He and Ne based fluorine gas mixtures.

B. Discharge chamber/charging scheme

Our aim was to homogeneously pump a 40 × 5 × 5 cm^3 volume of a KrF gas mix. The cross-sectional view of the discharge chamber accommodating this condition is shown in Fig. 4. The upper (cathode) and lower (anode) electrodes together with the electrode-holder plates are made of aluminum. The cathode is a flat electrode, while the anode is designed to homogeneously pump (to ensure homogeneous E-field distribution over) a 5 × 5 cm^2 region (marked by dashed lines). The insulator—forming the side walls of the chamber—is made of polivinyledene fluoride (PVDF). Three possible positions of the x-ray tubes are indicated in Fig. 4 (marked by I, II, and III), corresponding to that used in our experiments. Position I is a central preionization through the cathode electrode, position II is two-side preionization through the side walls, while position III is a twin source preionization through the cathode. In order to make the discharge area "accessible" to x rays from different directions, windows are milled out both on the side walls and on the upper electrode (electrode holder plate). The geometry of these windows is also seen in Fig. 4, allowing the irradiation of the pumped volume from the two sides, and from above in a large solid angle

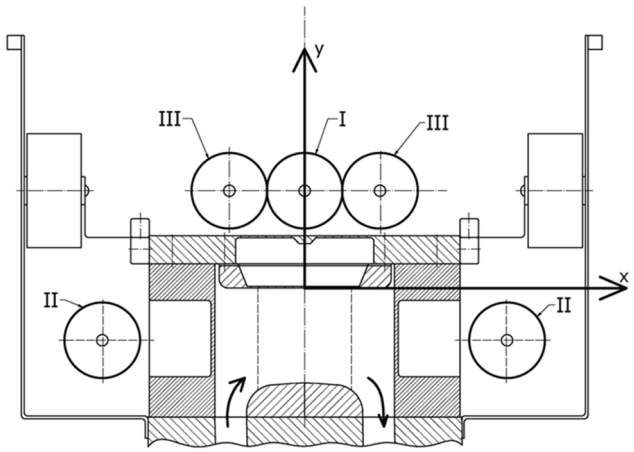

FIG. 4. Cross-sectional view of the discharge chamber allowing x-ray preionizations of different (I, II, III) geometries (for further details see the text).

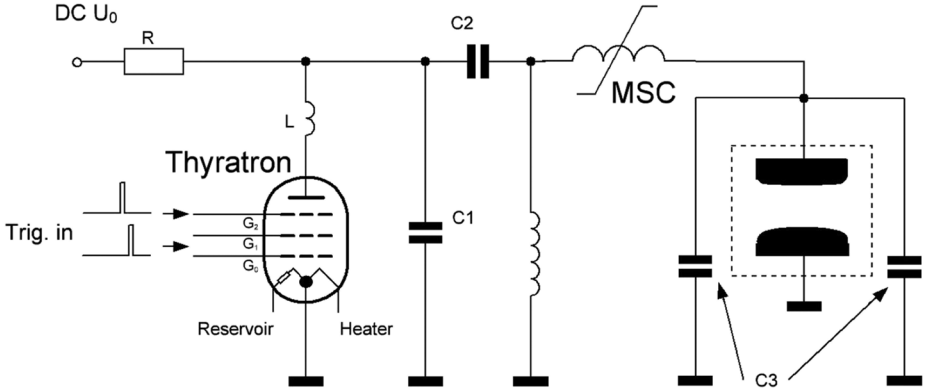

FIG. 5. Schematics of the L-C inversion and magnetic switch compressor (MSC) based charging circuit.

(in the latter case even allowing the use of two x-ray sources). The remaining thickness of the windows is 1 mm and 0.7 mm for PVDF and aluminum, respectively. The windows are segmented along the axis perpendicular to the figure in order to maintain the mechanical stability of the chamber. The ratio of the dimensions of the windows and that of the columns (bars) in between the windows are 12 mm/6 mm and 98 mm/2 mm for the PVDF walls and for the aluminum electrode holder plate, respectively. The electrode is not segmented, and it contains several holes on the side to ensure pressure equalization between the two sides of the cathode electrode; therefore, no bending of the surface. It is, however, the electrode holder plate, which has to wear the pressure difference of several bars. In the case of position III of the x-ray tubes, the dimension of the window is made even larger to accept x-ray radiations from two separate cylindrical x-ray guns (detailed explanation given later). In order to maintain the pressure durability of this component, in this case, another column (metal-bar) is left in the middle of the window (see the figure).

The position of the peaking capacitors (C_3 in Fig. 5) is also shown in Fig. 4, which was chosen to leave enough room for the x-ray guns for irradiation of the pumped volume both from the side and from the above. The laser chamber was connected to a gas reservoir/circulating fan (Lambda Physik Göttingen GmbH) allowing efficient transversal gas circulation in the chamber (indicated by arrows in the figure), thus, promoting high rep-rate operation.

In order to identify the different positions of the preionizers, a coordinate-system—centered to the axis of the cathode electrode as used in our calculations—is also shown in the figure. For the characterization of the positions of the x-ray guns—arranged always symmetrically to the y axis—their horizontal spatial separation ($\Delta x = 2\times$) and their y coordinates are used (for further details, see Sec. III).

The electric charging circuit—shown in Fig. 5—is a standard, thyratron (CX1573C, E2V Technologies) driven L-C inversion circuit, completed by a magnetic switch compressor (MSC) technology. For the given value of the main capacitor bank ($C_1 = C_2 = 196$ nF, determined by the electric energy to be transferred), the inversion time is synchronized to the switching of MSC by proper choice of L and of the cross section of the core of the MSC (Metglas 2605 Co) surrounded by a "spatially distributed coil" of one winding. The peaking capacitance $C_3 = 50$ nF is equally distributed along the two sides of the discharge chamber (see also Fig. 4). With the use of this charging circuit, a 60 kV electric pulse of 120 ns rise time could be produced on the cathode electrode, at a power supply voltage of $U_0 = 32$ kV.

The temporal behavior of this pulse (curve U) is shown in Fig. 6 at $U_0 = 30$ kV. Curve I is the discharge current, which is picked up by six turn coils of 0.3 cm^2 cross section, inserted into the discharge loop (between C3 and the discharge chamber).

The short duration of the preionization process and that of the main discharge requires the exact synchronization of the two charging circuits, including the compensation of their long-term drift (mainly initiated by the thyratrons). For this purpose, an automatic synchronization unit—based on optical fiber communication—was developed to compensate for the long-term drift in 5 ns steps. This device monitors the time difference between the signals coming from the current probes of preionization and the main discharge, then, properly changes the starting point of preionization until the preset condition is reached. With regard to the relatively narrow temporal width of the x-ray pulse and that of the main discharge, 5 ns temporal resolution of the synchronization revealed to be necessary.

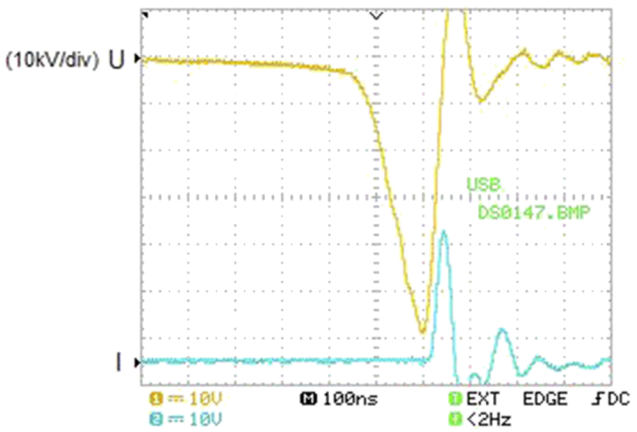

FIG. 6. Temporal behavior of the electric pulse measured on the cathode electrode (curve U) and of the discharge current (curve I).

In the case of all the following comparative measurements, the same gas mixtures were used (120 mbar He with 5% F_2, 150 mbar Kr filled up to 2.0 bars with He). We are aware of the fact that Ne-based mixtures are better suited for x-ray preionization due to the nearly 10 times higher ionization rate of Ne compared to He.[18] The reason for the use of He buffer gas in these experiments is two-fold: the sensitivity of the spatial distribution of the discharge when compared to that of the preionization is more pronounced (therefore can better be measured) when preionization is not in deep saturation; moreover, our aim was to reach the limit of saturation even with the less appropriate (but less expensive) He.

Another practical consequence of the use of the proposed electric charging circuits (both for preionization and for pumping the main discharge) is that relatively low (<35 kV) initial DC voltage and corresponding power supplies are satisfactory; due to the 1:4 pulse transformers and the L-C inversion charging circuit, higher voltages are only present in the restricted parts of the system, and only for a limited time (≤100 ns). This significantly relaxes the isolation issues/requirements leading to practical design of easy and reliable operation.

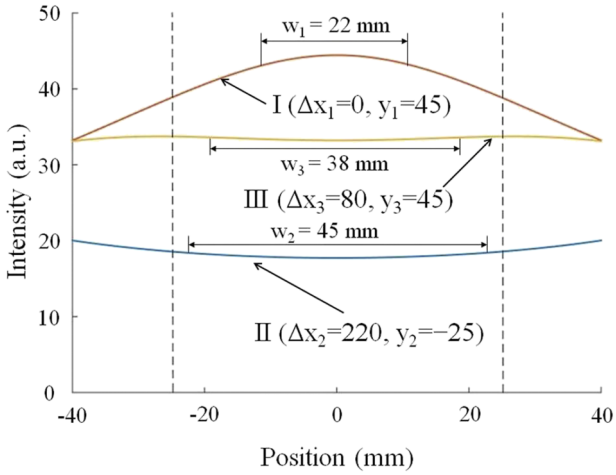

FIG. 7. Calculated distribution of the x-ray intensity, when preionization is done (I) by one x-ray source from above (through the electrode), (II) by two x-ray sources from two sides (through the walls), and (III) by two x-ray sources, properly positioned above the cathode electrode. Along the curves, the experimentally obtained discharge widths (w) are also indicated.

III. RESULTS

A. Spatial distribution of the x-ray field of preionization

In this section, the results of our numerical calculations and of corresponding measurements for the spatial distribution of the x-ray intensity for different preionization geometries are presented. Since the absorption of x rays in the KrF gas mixture is weak, its contribution to the spatial distribution and to the spectral behavior of the x-ray can be neglected. In our calculations, the absorptions in the windows of the side walls and of the upper electrode are also excluded; based on their similar value, they had no practical contribution to the normalized (relative) intensity of the calculated x-ray fields (including the spectral behavior).

Based on the cylindrical emission geometry of the x-ray sources, r^{-1} spatial dependence of the x-ray intensity and no spectral changes were assumed/used in our calculations. Three different x-ray tube positions were considered; arrangement *I* represents preionization of a single source (of double intensity) from above (where the x-ray source is characterized by $\Delta x_1 = 0$, $y_1 = 45$). The corresponding horizontal x-ray distribution along the x axis (at the surface of the cathode) is shown in Fig. 7 by curve I. This curve shows a pronounced maximum in the middle of the electrode, leading to a relatively narrow discharge ($w_1 \approx 22$ mm is measured in our experiments) centered to the middle of the electrodes. The width of the discharge is also indicated along curve I of Fig. 7. Arrangement II (a preionization from two sides, by two x-ray guns of $\Delta x_2 = 220$, $y_2 = -25$, through the chamber walls) results in an x-ray distribution of "opposite" tendency, having an intensity minimum in the middle, as shown in Fig. 7 by curve II. In this arrangement, the experimentally observed discharge width was significantly broadened to $w_2 \approx 45$ mm, however, containing a less-pumped dip in the middle.

The width of the discharge even in this case "remained" still inside the dashed lines of Fig. 7, which confine that area where homogeneous discharge is expected (the E-field distribution is homogeneous). Basic geometrical considerations suggest that two x-ray sources positioned above the cathode (corresponding to arrangement III in Fig. 4) can produce a spatial distribution whose spatial characteristics are expected in between the former two (including the possibility to form a homogeneous spatial distribution). This is clearly seen in curve III of Fig. 7, for $\Delta x_3 = 80$ and $y_3 = 45$ setting of the two preionizers. In this case, the spatial distribution of preionization is flat, leading to a homogeneous discharge of $w_3 = 38$ mm width.

When this active medium is surrounded by a plane-parallel resonator (consisting of a HR back mirror and an uncoated MgF_2 window), the spatial distribution of the output beam—measured some 60 cm away from the output window of the discharge chamber—is shown in Fig. 8. For reference, a rectangular area of 52×38 mm^2 dimensions is also indicated in the figure by dashed lines.

In Fig. 9, the calculated horizontal distribution of the x-ray intensity for the same ($\Delta x_3 = 80$, $y_3 = 45$) position of the two cylindrical x-ray sources is shown by solid lines in different horizontal planes through the discharge volume (for different values of y). The shape of the curves changes from convex to concave (through a flat distribution) as y changes. The two dashed lines confine again the region where homogeneous pumping is provided. Most homogeneous preionization seems to be best fulfilled in a plane characterized by $y = -10$ (10 mm below the cathode electrode).

All these calculations were confirmed by measurements. The spatial dependence of the x-ray intensity along the x axis was measured for different y values—in a geometrical configuration corresponding to position III of the x-ray tubes (Fig. 4) —in an independent experiment. This measurement was performed without (outside) the discharge chamber, using the two x-ray guns and the RD15 photodiode-amplifier based detector. The relative positions of the x-ray tubes and of the detector were "converted" to the coordinate system shown in Fig. 4. The measured x-ray intensities were

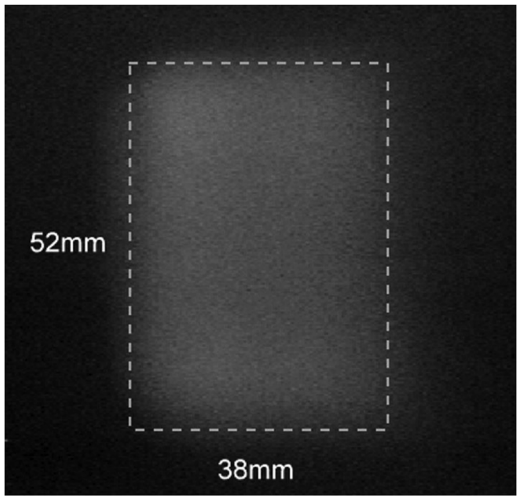

FIG. 8. Spatial distribution of the output beam corresponding to x-ray tube position III.

normalized to have optimum matching to the theoretical curves at x = 0 and y = 10. In this way, the points in Fig. 9 are the measured x-ray intensity distributions in different horizontal planes corresponding to that of the calculated curves. Good matching of the theoretical and experimental curves is visible. In the near vicinity of the x-ray sources (for positive values of y), the spatial modulation of the measured distribution is more pronounced compared to the calculated values. This is due to the slight angular dependence of the radiation of the x-ray guns, which was disregarded in the calculations. The dependence of the sensitivity of the photodiode on the incidence angle of the radiation was also neglected. This measurement, however, clearly confirmed that the spatial distribution changes from convex to concave when moving closer to a twin, line-emitting radiation source.

It is a reasonable assumption that along the electric field vectors in the pumped area (along the y axis in Fig. 4), it is the integral (or the average value) of the x-ray field strength, which determines the (integrated) effect of preionization for a fixed value of x. It is known from the former studies that the influence of the spatial distribution of preionization on that of the discharge is most pronounced in the vicinity of the cathode,[18] which would then require a y-dependent weighting factor during integration/averaging. In our present approach, this effect was disregarded; integration was performed without any weighting factor. The result of calculations based on such averaging is shown in Fig. 10, where the distributions corresponding to different values of y (seen in Fig. 9) are averaged between the electrodes (between y = 0 and y = −50). The curves marked by $\Delta x_3 = 80$ and $y_3 = 45$ in Fig. 10 correspond to the initial (formerly assumed) positions of the x-ray guns, which turned to be very close to the optimum, flat distribution. It is also seen from the curves that by changing (symmetrically) the horizontal positions of the x-ray sources (changing their Δx_3 horizontal separation from 70 mm to 100 mm), the "integrated" distribution can be tuned to either concave or to convex. This is clearly visible on the enlarged intensity scale of Fig. 10. The main claim of these considerations is that using line-emitting x-ray sources of cylindrical emission geometry, even in the near vicinity of the discharge volume, homogeneous (integrated) x-ray distribution can be achieved along the axis perpendicular to the E-field. This offers to fulfill the most important necessary condition for homogeneous energy deposition by the discharge. Moreover, by changing the horizontal spatial separation of the x-ray sources, easy tuning can be realized; either the middle or the outer sections of the discharge volume are irradiated more intensively, which can compensate for eventual inhomogeneities of the E-field of excitation, thus, the desired discharge geometry can be produced in a technically simple way.

Since the spatial distribution of the E-field is a critical function of the shape and separation of the electrodes, of the surrounding discharge loop,[15] and/or of the skin-effect,[20] the preionization-based spatial tuning of the discharge[20] is of great practical importance.

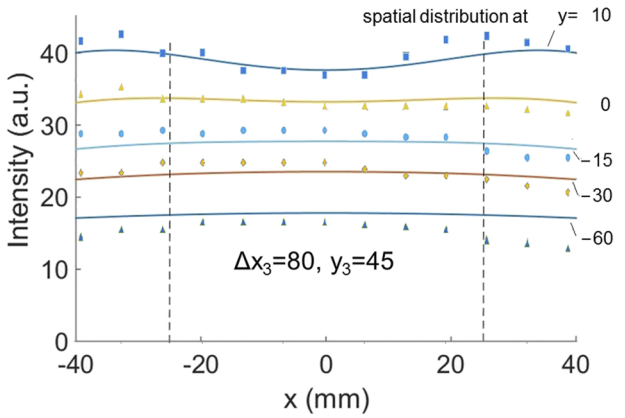

FIG. 9. Calculated distribution of the x-ray field (solid lines) along the x axis for different values of y, corresponding to arrangement III (when the position of the x-ray guns is $\Delta x_3 = 80$, $y_3 = 45$). The points are measured values corresponding to the calculated curves.

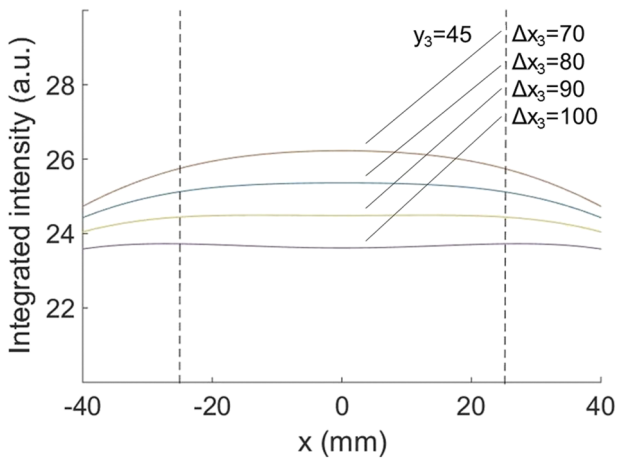

FIG. 10. Calculated "integrated" x-ray field distributions between the electrodes for different horizontal separations of the x-ray sources.

IV. CONCLUSION

In conclusion, an x-ray preionized, short-pulse KrF excimer amplifier is developed. As a part of this activity, a short-pulse, twin, cylindrical x-ray gun is realized, which fulfills the needs of an efficient preionization of fluorine-based gas mixtures, with regard to its temporal, spatial, and intensity requirements.

It is shown both theoretically and experimentally that the radiation of the x-ray sources—even in the close vicinity of the discharge volume (which is a necessary condition for intense irradiation)—can result in homogeneous preionization by proper choice of their positions. Moreover, by a slight change in the positions of the x-ray guns, the maximum strength of preionization can be fine-tuned either to the middle or to the side of the discharge, which can be used as a fine-compensation of the eventual inhomogeneities of the E-field of pumping.

As a result of this fine-tuning of preionization, the amplifier exhibits excellent spatial homogeneity, characterized by a 5 × 3.8 cm^2 discharge cross section.

ACKNOWLEDGMENTS

This work was supported by the Hungarian Scientific Research Fund (OTKA113222) and by the European Social Fund (EFOP-3.6.2-16-2017-00005—Ultrafast physical processes in atoms, molecules, nanostructures, and biological systems). We are grateful for the support from Hungary Grant No. TUDFO/47138-1/2019-ITM FIKP of the Ministry of Innovation and Technology. The author thanks E. Müller-Horsche (Hochshule Augsburg), Ya. E. Krasik (Israel Institute of Technology), and G. Firla (VAC GmbH, Germany) for valuable discussions; B. Gilicze for performing the numerical calculations; and L. Gyihor for his participation in some parts of this R&D activity. The technical assistance of R. Bognár, Z. Szántó, B. Csánk, and R. Dajka is also acknowledged.

REFERENCES

[1] S. Szatmári, G. Marowsky, and P. Simon, *Landolt–Börnstein—Group VIII 1B1*, edited by G. Herziger, H. Weber, and R. Poprawe (Springer, 2007), p. 215.
[2] A. B. Borisov, J. C. McCorkindale, S. Poopalasingam, J. W. Longworth, P. Simon, S. Szatmári, and C. K. Rhodes, Rep. Prog. Phys. **79**, 046401 (2016).
[3] M. Martinez, W. Bang, G. Dyer, X. Wang, E. Gaul, T. Borger, M. Ringuette, M. Spinks, H. Quevedo, A. Bernstein, M. Donovan, and T. Ditmire, AIP Conf. Proc. **1507**, 874 (2012).
[4] F. Wagner, C. P. João, J. Fils, T. Gottschall, J. Hein, J. Körner, J. Limpert, M. Roth, T. Stöhlker, and V. Bagnoud, Appl. Phys. B **116**, 429 (2014).
[5] T. M. Jeong and J. Lee, Ann. Phys. **526**, 157 (2014).
[6] Y. Chu, X. Liang, L. Yu, Y. Xu, L. Xu, L. Ma, X. Lu, Y. Liu, Y. Leng, R. Li, and Z. Xu, Opt. Express **21**, 29231 (2013).
[7] S. Szatmari and P. Simon, Opt. Commun. **98**, 181 (1993).
[8] S. Szatmári and F. P. Schäfer, Opt. Commun. **68**, 196 (1988).
[9] S. Szatmári, F. P. Schäfer, E. Müller-Horsche, and W. Müchenheim, Opt. Commun. **63**, 305 (1987).
[10] R. Nodomi, Y. Oeda, K. Sajiki, S. Nakajima, M. Watanabe, and S. Watanabe, IEEE J. Quantum Electron. **27**, 441 (1991).
[11] G. Almàsi, S. Szatmàri, and P. Simon, Opt. Commun. **88**, 231 (1992).
[12] S. Szatmári, G. Almási, and P. Simon, Appl. Phys. B **53**, 82 (1991).
[13] S. Szatmári and F. P. Schäfer, J. Opt. Soc. Am. B **4**, 1943 (1987).
[14] H. Mizoguchi, A. Endoh, J. Jethwa, B. Rácz, and F. P. Schäfer, Appl. Phys. B **52**, 195 (1991).
[15] G. Kovacs and S. Szatmari, Meas. Sci. Technol. **5**, 127 (1994).
[16] H. Shields, SPIE Proc. **1046**, 15 (1989).
[17] C. Tallman, SPIE Proc. **1046**, 2 (1989).
[18] K. Midorikawa, M. Obara, and T. Fujioka, IEEE J. Quantum Electron. **20**, 198 (1984).
[19] M. Steyer, J. Phys.: Appl. Phys. **23**, 18 (1990).
[20] M. S. Pronko, IEEE J. Quantum Electron. **30**, 2147 (1994).
[21] Ya. E. Krasik, D. Yarmolich, J. Z. Gleizer, V. Vekselman, Y. Hadas, V. Tz. Gurovich, and J. Felsteiner, Phys. Plasmas **16**, 057103 (2009).
[22] J. Z. Gleizer, T. Queller, Yu. Bliokh, S. Yatom, V. Vekselman, Ya. E. Krasik, and V. Bernshtam, J. Appl. Phys. **112**, 023303 (2012).